SCIENCE CHINA
Information Sciences

• RESEARCH PAPER •

March 2025, Vol. 68, Iss. 3, 132205:1–132205:14
https://doi.org/10.1007/s11432-024-4142-1

An enhanced equivalent input disturbance approach to current control of PMSM with periodic and aperiodic disturbances

Tao YANG[1], Youwu DU[1*], Bo LI[1], Weihua CAO[2], Chuanke ZHANG[2] & Jinhua SHE[3]

[1]*School of Electrical & Information, Jiangsu University of Technology, Changzhou 213001, China*
[2]*School of Automation, China University of Geosciences, Wuhan 430074, China*
[3]*School of Engineering, Tokyo University of Technology, Tokyo 192-0982, Japan*

Received 6 May 2024/Revised 25 July 2024/Accepted 30 August 2024/Published online 8 February 2025

Abstract The current-loop control of a permanent magnet synchronous motor (PMSM) system suffers from periodic and aperiodic disturbances, which result in current ripples and degrade control performance. This paper presents an enhanced equivalent-input-disturbance (EID) approach to reject periodic and aperiodic disturbances in the current loop of a PMSM. Two additional quasi-resonant compensators (QRCs) are integrated into a conventional EID estimator with a low-pass filter (LPF) to handle the disturbances. The configuration of an enhanced EID (EEID)-based control system for PMSM current loop is explained. An analysis in the frequency domain shows the mechanism of the presented method for rejecting periodic and aperiodic disturbances simultaneously. It reveals that the sensitivity reduction of the system for aperiodic disturbances is mainly determined by the bandwidth of the LPF and that for periodic disturbances is determined by the parameters of the QRCs. The stability of the system is analyzed using the Nyquist stability criterion. The design algorithm for system parameters is provided. Compared to the conventional EID approach, the proposed method provides an additional degree of freedom to deal with periodic disturbances. The design of the QRCs is independent of each other, which makes the proposed method flexible and easy to implement. The effectiveness and the superiority of the EEID approach are validated by simulation results of a PMSM system.

Keywords equivalent input disturbance (EID), disturbance rejection, permanent magnet synchronous motor (PMSM), periodic and aperiodic disturbances, quasi-resonant compensator

Citation Yang T, Du Y W, Li B, et al. An enhanced equivalent input disturbance approach to current control of PMSM with periodic and aperiodic disturbances. Sci China Inf Sci, 2025, 68(3): 132205, https://doi.org/10.1007/s11432-024-4142-1

1 Introduction

The requirement for the accuracy control of permanent magnet synchronous motors (PMSMs) is becoming increasingly urgent in many industrial systems, especially in high-performance servo systems [1–3]. There are several disturbances including current measurement errors, inverter dead times, flux harmonics, and parameter variations in PMSM drive systems, which hinder improving control performance [4,5]. Disturbance rejection becomes an essential objective in the design of a PMSM drive system. However, it is still a challenge due to the large frequency range of the disturbances. According to the characteristics of the disturbances, they can be divided into two categories: periodic and aperiodic disturbances. These disturbances cause both periodic and aperiodic current ripples in the current loop of a PMSM drive system and then degrade control performance [6]. It is necessary to explore new control strategies that suppress both periodic and aperiodic disturbances.

Several composite schemes have been proposed to handle both aperiodic and periodic disturbances in recent years [7–9]. They share a similar mechanism, that is, aperiodic disturbances are estimated and rejected by an inner-loop estimator or observer, such as a disturbance observer (DOB) [10], an equivalent-input-disturbance (EID) estimator [11,12], and an extended state observer (ESO) [13,14], while periodic disturbances are suppressed by the feedback control, for example, repetitive control (RC) [15], resonant control [16], and iterative learning control [17]. An extended repetitive controller was proposed to suppress current harmonics caused by inverter dead times [15]. An improved EID estimator was

* Corresponding author (email: duyouwu@jsut.edu.cn)

presented to reject periodic disturbances by combining the RC and the EID approach (RC-EID) [18]. It integrated the internal model of a periodic disturbance in an EID estimator and thus suppressed the periodic disturbance without a steady error. Mohanapriya et al. [19] first used a repetitive controller to track a periodic reference. Then, combined the EID approach with the Smith predictor to reject the effect of stochastic disturbances and time delays. The active disturbance rejection control (ADRC) combined with a resonant controller was used to suppress harmonic disturbances in a system [20]. In [21], proportional-integral resonant controllers were applied to direct torque-controlled PMSM drive systems to suppress the 2nd and 6th fundamental frequency harmonics. In [22], an iterative learning ADRC method was proposed for piezoelectric actuators to suppress aperiodic and periodic disturbances and improve the robustness and tracking performance of actuators. The above schemes suppress periodic disturbances mainly by the feedback control, which is an outer loop. Since it has been acknowledged in the literature that an inner loop is a more effective way to reject disturbances, there is room for improving the performance of rejecting periodic disturbances.

This paper presents an alternative, simple way to handle periodic and aperiodic disturbances for a PMSM system using the EID approach combined with quasi-resonant compensators (QRCs) [23]. The EID approach is a commonly used active disturbance-rejection method, which consists of a state observer and an EID estimator. It uses a low-pass filter (LPF) to filter out measurement noise and obtain a causal estimate for compensation on the control input channel. However, the estimate of a disturbance with frequencies outside the bandwidth of the filter cannot pass through it. Thus, there is a limitation on disturbance rejection for periodic disturbances with high frequencies, which leads to poor control performance. In this study, an enhanced EID (EEID) estimator is developed to remove the limitation by integrating QRCs in the conventional EID estimator. First, the control problem of the current loop of a PMSM is formulated. An analysis is provided to show the limitation of the conventional EID approach concerning periodic and aperiodic disturbances. Next, the configuration of an EEID-based control system for the current loop of a PMSM is given. Two QRCs are used to handle two periodic disturbances in the EEID estimator. The mechanism of the disturbance rejection is analyzed. It shows that the EEID approach is capable of rejecting periodic and aperiodic disturbances simultaneously. Specifically, the QRCs are designed to compensate for the periodic disturbances, while an LPF is used to handle aperiodic disturbances. Then, stability analysis and design procedure indicate that the system design is simple. Finally, simulations on a PMSM system are carried out and three other methods are used for comparison with the presented method. Simulation results demonstrate the validity and effectiveness of the EEID approach. The main contribution of this study is as follows.

(1) Two QRCs are integrated into the conventional EID estimator to enhance disturbance-rejection performance for periodic disturbances. The presented EEID estimator is capable of rejecting periodic and aperiodic disturbances simultaneously.

(2) The design and analysis of an EEID-based control system show that the design of the QRCs and EID estimator is independent of each other. Periodic and aperiodic disturbances are handled by QRCs and the EID estimator, respectively. Moreover, QRCs behave like a patch to the EID estimator. As a result, the proposed method is flexible in system design and easy to implement.

(3) The stability of the presented EEID approach is analyzed using the Nyquist stability criteria. The disturbance-rejection mechanism is systematically explained using the separation theorem. The parameter-tuning procedure is discussed in detail.

2 Problem formulation

2.1 Dynamic model of PMSM

The dynamic model of a surface-mounted PMSM in the d-q frame is [24]

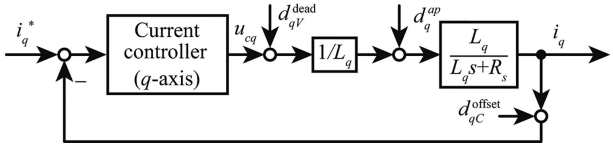

Figure 1 Distribution of multi-source disturbances in the q-axis current loop.

$$\begin{cases} \dfrac{\mathrm{d}i_d}{\mathrm{d}t} = \dfrac{1}{L_d}u_d - \dfrac{R_s}{L_d}i_d + \dfrac{L_q}{L_d}p_n\omega_m i_q, \\ \dfrac{\mathrm{d}i_q}{\mathrm{d}t} = \dfrac{1}{L_q}u_q - \dfrac{R_s}{L_q}i_q - p_n\omega_m\left(\dfrac{L_d}{L_q}i_d + \dfrac{1}{L_q}\psi_f\right), \\ \dfrac{\mathrm{d}\omega_m}{\mathrm{d}t} = \dfrac{1}{J}(T_e - T_L - B_s\omega_m), \\ T_e = \dfrac{2}{3}p_n[\psi_f i_q + (L_d - L_q)i_d i_q], \end{cases} \tag{1}$$

where u_d and u_q are stator voltages; i_d and i_q are stator currents; R_s, ψ_f, and ω_m are the stator resistance, magnetic flux linkage, and the rotor speed, respectively; L_d and L_q are stator inductances; J is the moment of the inertial; T_e is the electromagnetic torque; T_L is the load torque; B_s is the frictional coefficient; and p_n is the number of poles.

There are several nonlinearities in PMSM drive systems, such as magnetic chain harmonics, dead times of inverters, and measurement errors in current. These nonlinearities can be viewed as an internal disturbance. In general, the control strategy of "$i_d = 0$" is usually used in the current loop. Thus, the dynamics in the current loop can be rewritten as

$$\frac{\mathrm{d}i_q}{\mathrm{d}t} = b_q u_q + d_q^{\mathrm{total}}, \tag{2}$$

where $b_q = 1/L_q$ and d_q^{total} is a total disturbance including nonlinearities. It can be denoted by

$$d_q^{\mathrm{total}} = d_q^p + d_q^{\mathrm{ap}}, \tag{3}$$

where

$$d_q^{\mathrm{ap}} = -\frac{R_s}{L_q}i_q - \frac{1}{L_q}p_n\omega_m\psi_f, \tag{4}$$

and d_q^p represents the periodic disturbance in the q-axis. The periodic disturbance d_q^p is mainly caused by the dead times of inverters and measurement errors in current [6]. It is given by

$$d_q^p = d_{\mathrm{qV}}^{\mathrm{dead}} + d_{\mathrm{qC}}^{\mathrm{offset}}, \tag{5}$$

where

$$\begin{cases} d_{\mathrm{qV}}^{\mathrm{dead}} = \displaystyle\sum_{i=0}^{\infty} d_{\mathrm{qi}}\cos(6i\theta_e), \\ d_{\mathrm{qC}}^{\mathrm{offset}} = d_{\mathrm{off}}\cos(\theta_e + \alpha). \end{cases} \tag{6}$$

The parameters d_{qi} and d_{off} are the amplitudes of $d_{\mathrm{qV}}^{\mathrm{dead}}$ and $d_{\mathrm{qC}}^{\mathrm{offset}}$, respectively; α is the constant angular displacement; and θ_e is the electrical angle. These periodic components cause the pulsations of the speed of a PMSM, which are mainly composed of the 1st and 6th electrical frequencies. The distribution of disturbances in the q-axis current loop is shown in Figure 1.

2.2 Preliminaries: EID approach

The basic concept of the EID approach is to convert the effect of a disturbance on the output of a system into the effect of a fictitious signal that is imposed on the control input channel. The fictitious signal is called an EID. A state observer and an EID estimator are designed to calculate an estimate of the EID in a real-time fashion. The estimate is then incorporated into the control input to compensate for the

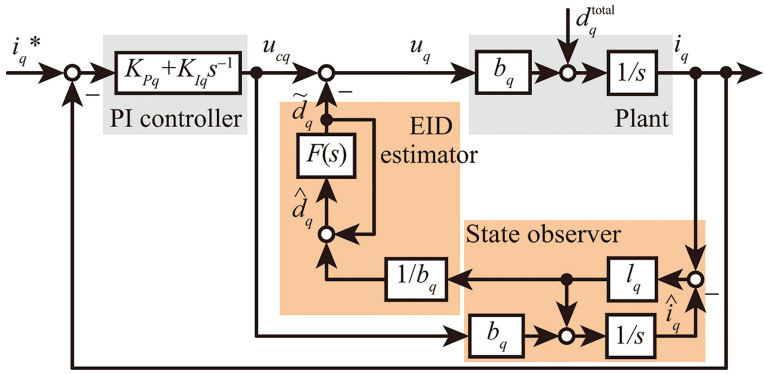

Figure 2 (Color online) Block diagram of EID-based control scheme for the q-axis current loop.

effect of the external disturbance. Figure 2 illustrates the block diagram of an EID-based control scheme for the q-axis current loop. The mechanism of disturbance estimation is explained as follows.

Rewrite (2) as

$$\frac{\mathrm{d}i_q}{\mathrm{d}t} = b_q(u_q + d_{\mathrm{qe}}^{\mathrm{total}}), \tag{7}$$

where $d_{\mathrm{qe}}^{\mathrm{total}} = d_q^{\mathrm{total}}/b_q$. The state observer is designed as

$$\frac{\mathrm{d}\hat{i}_q}{\mathrm{d}t} = b_q u_{\mathrm{cq}} + l_q(i_q - \hat{i}_q), \tag{8}$$

where u_{cq} and l_q are the input and the gain of the observer, respectively; $\hat{i}_q$ is the estimate of the current. Letting

$$\Delta i_q = \hat{i}_q - i_q, \tag{9}$$

and substituting it into (7) yield

$$\frac{\mathrm{d}\hat{i}_q}{\mathrm{d}t} = b_q u_q + \left(b_q d_{\mathrm{qe}}^{\mathrm{total}} + \frac{\mathrm{d}\Delta i_q}{\mathrm{d}t}\right). \tag{10}$$

Assume that there exists a control input Δd_q that satisfies

$$\frac{\mathrm{d}\Delta i_q}{\mathrm{d}t} = b_q \Delta d_q. \tag{11}$$

Substituting (11) into (10) and letting the estimate of the EID be

$$\hat{d}_q = d_{\mathrm{qe}}^{\mathrm{total}} + \Delta d_q \tag{12}$$

allows us to express the plant as

$$\frac{\mathrm{d}\hat{i}_q}{\mathrm{d}t} = b_q(u_q + \hat{d}_q). \tag{13}$$

Combining (8) and (13) yields

$$b_q(\hat{d}_q + u_q - u_{\mathrm{cq}}) = l_q(i_q - \hat{i}_q). \tag{14}$$

If we solve (14) for $\hat{d}_q$, then an estimate of the EID is

$$\hat{d}_q = \frac{1}{b_q} l_q(i_q - \hat{i}_q) + u_{\mathrm{cq}} - u_q, \tag{15}$$

where u_q is the input of the plant.

The conventional EID approach uses an LPF to filter out high-frequency components of the estimate and obtain a casual estimate for compensation in the control law. The filter is

$$F(s) = \frac{\omega_q}{s + \omega_q}, \tag{16}$$

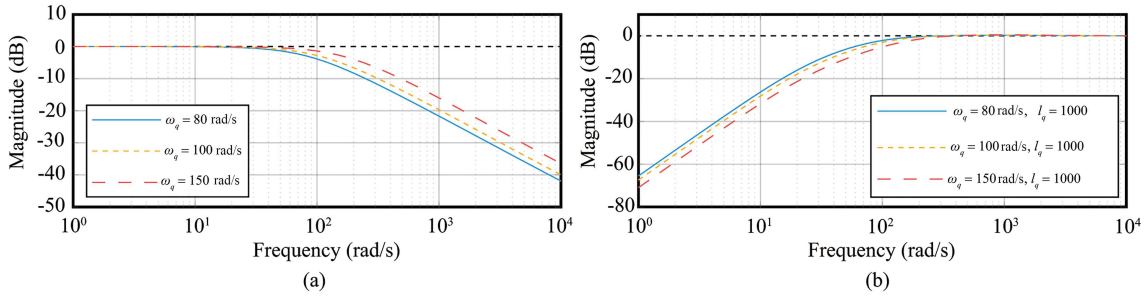

Figure 3 (Color online) Frequency responses of (a) filter $F(s)$ and (b) sensitivity function $S_{\rm EID}(s)$.

where ω_q is the cut-off angular frequency of the filter. To ensure the accuracy of disturbance estimation, the following frequency characteristics should be satisfied

$$| F(\mathrm{j}\omega) | \approx 1, \quad \forall \omega \in [0, \omega_{\rm ar}], \tag{17}$$

where $\omega_{\rm ar}$ is the highest angular frequency of the disturbance. In general, the cut-off angular frequency of $F(s)$ is usually set to be $\omega_q \geqslant 5\omega_{\rm ar}$. The filtered estimate $\tilde{d}_q$ is used to compensate for the disturbance in the control law

$$u_q = u_{\rm cq} - \tilde{d}_q. \tag{18}$$

The conventional EID approach uses the LPF to guarantee the accuracy of disturbance estimation in a predefined frequency band. Theoretically, as long as a disturbance with frequencies stays within the band, it can be well estimated and compensated. However, a disturbance with frequencies outside the band will be filtered out, which leads to poor disturbance-rejection performance. Therefore, the conventional EID approach is weak in suppressing medium-and-high-frequency periodic disturbances. On the other hand, if the bandwidth of the filter is expanded to include the frequencies of those disturbances, the estimate will be sensitive to high-frequency noise and may cause the instability of the system. This problem is analyzed in terms of the Bode diagram as follows.

From Figure 2, the sensitivity function for disturbance estimation is

$$S_{\rm EID}(s) = \frac{s^2 + l_q s}{s^2 + l_q s + l_q \omega_q}. \tag{19}$$

Figure 3 shows the frequency responses of the sensitivity function $S_{\rm EID}(s)$ and the filter $F(s)$ with different values of ω_q. It can be seen that expanding the bandwidth of the filter reduces the sensitivity of the system in the low and medium frequencies at the price of increasing the sensitivity to the high frequencies. However, there are medium-and-high-frequency periodic disturbances in the PMSM current loop, such as measurement errors in current and dead times of inverters, which cause current ripples and degrade control performance. Therefore, it is necessary to explore how to improve the conventional EID estimator to enhance the suppression capability of periodic and aperiodic disturbances simultaneously.

3 Design and analysis of EEID-based control scheme for PMSM current loop

There is a limitation on disturbance rejection for the conventional EID estimator in the presence of periodic disturbances with high frequencies. This study overcomes the limitation by combining the EID estimator with the QRC, which has been widely used for harmonic suppression in recent years. This section describes the design and analysis of an EEID estimator, which is capable of handling aperiodic and periodic disturbances simultaneously.

3.1 Design of EEID-based control scheme

To reject the current measurement errors and dead times of the inverter, two QRCs with different resonant frequencies are designed to compensate for these two disturbances separately. An EEID estimator is developed to handle the periodic disturbances $d_{\rm qV}^{\rm dead}$ and $d_{\rm qC}^{\rm offset}$ in the current loop of a PMSM by integrating two QRCs into a conventional EID estimator. Figure 4 shows the block diagram of the EEID-based control scheme for the q-axis current loop. The EEID estimator provides two degrees of freedom to handle

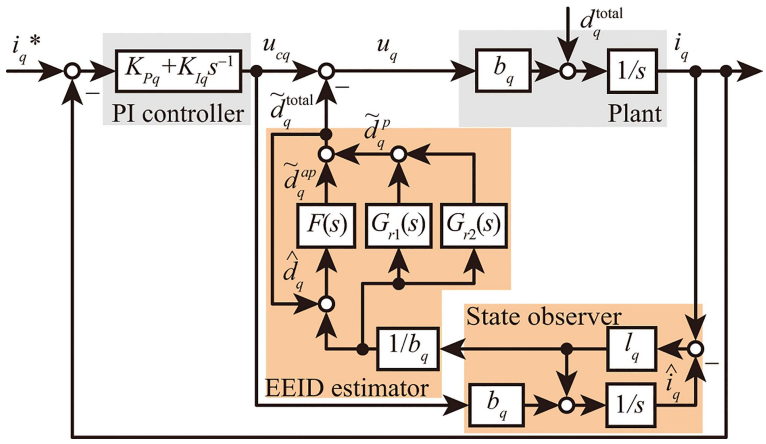

Figure 4 (Color online) Block diagram of EEID-based control scheme for the q-axis current loop.

disturbances: the LPF $F(s)$ is used to estimate low-frequency disturbances and the two QRCs ($G_{r1}(s)$ and $G_{r2}(s)$) are used to estimate periodic disturbances with frequencies within the bandwidth of the QRCs. As a result, the EEID estimator is able to estimate both aperiodic and periodic disturbances. In addition, it is easy to extend the proposed scheme to control systems with multiple periodic disturbances by using multiple QRCs with the corresponding resonant frequencies.

The QRCs in this study are designed to be

$$\begin{cases} G_{r1}(s) = \dfrac{2K_r\omega_c s}{s^2 + 2\omega_c s + {\omega_{r1}}^2}, \\ G_{r2}(s) = \dfrac{2K_r\omega_c s}{s^2 + 2\omega_c s + {\omega_{r2}}^2}, \end{cases} \tag{20}$$

where K_r is the resonant coefficient; ω_c is the resonance bandwidth; ω_{r1} and ω_{r2} are the angular frequency of $d_{\text{qC}}^{\text{offset}}$ and $d_{\text{qV}}^{\text{dead}}$, respectively. For simplicity of design and analysis, the same K_r and ω_c are used in the two QRCs. The estimates of aperiodic and periodic disturbances are denoted by $\tilde{d}_q^{\text{ap}}$ and $\tilde{d}_q^{p}$, respectively. The control law of the system can be rewritten as

$$u_q = u_{\text{cq}} - \tilde{d}_q^{\text{total}} \tag{21}$$

by using the estimates, where $\tilde{d}_q^{\text{total}} = \tilde{d}_q^{\text{ap}} + \tilde{d}_q^{p}$.

Remark 1. The EEID approach integrates the QRCs into the conventional EID estimator, while the RC-EID method embeds the internal model of a periodic disturbance. Compared to the RC-EID method, the EEID approach is capable of rejecting periodic and aperiodic disturbances simultaneously. The design of the EEID estimator is flexible. QRCs act as a patch to the conventional EID estimator, which can be easily extended to handle multiple periodic disturbances. The performance of rejecting periodic and aperiodic disturbances can be tuned by the QRCs and EID estimator, respectively. As long as the frequencies of periodic disturbances stay within the bandwidth of QRCs, they can be effectively rejected. Moreover, more tuning parameters, such as the bandwidth and gain of the QRCs, ensure a wide range of applications of the presented method.

Remark 2. The presented method embeds the QRCs in the EID estimator to improve the performance of rejecting periodic disturbances. In the EEID estimator, the QRCs are designed to handle the periodic disturbances, while the LPF is used to deal with the aperiodic disturbances. Each QRC estimates a disturbance in a predefined frequency range by selecting the corresponding bandwidth. The design of the QRCs is independent of each other, which simplifies the system design. Since the QRCs behave like second-order filters, the computational complexity is low. As a result, the proposed EEID estimator is flexible in design and easy to implement.

3.2 Analysis of disturbance-rejection mechanism

Combining (7)–(9) and (21) yields

$$\frac{\mathrm{d}\Delta i_q}{\mathrm{d}t} = -l_q\Delta i_q - b_q\tilde{d}_q^{\text{total}}. \tag{22}$$

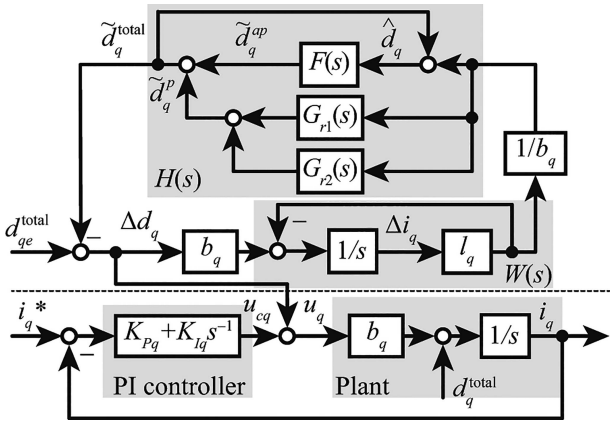

Figure 5 Equivalent block diagram of Figure 4.

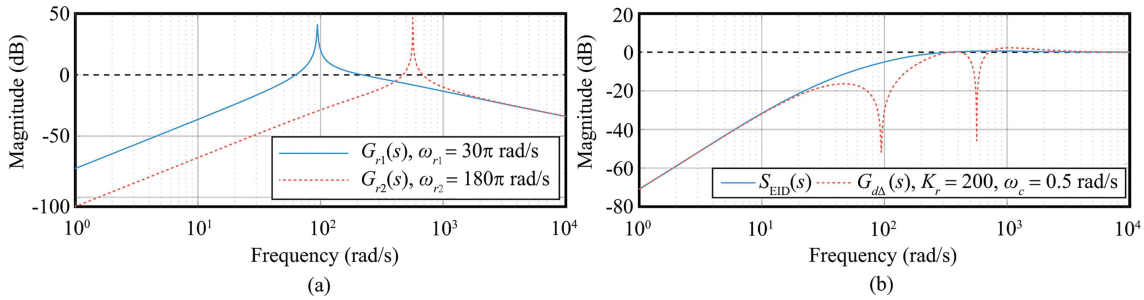

Figure 6 (Color online) Comparison of frequency responses for the conventional EID approach and the proposed scheme. (a) $G_{r1}(s)$ and $G_{r2}(s)$ and (b) $S_{\text{EID}}(s)$ and $G_{d\Delta}(s)$ with $l_q = 1000$, $\omega_q = 100$ rad/s.

Redraw Figure 4 as Figure 5 based on the (7), (9), (21), and (22).

Define

$$\begin{cases} W(s) = l_q(s + l_q)^{-1}, \\ H(s) = [F(s) + R(s)][1 - F(s)]^{-1}, \end{cases} \tag{23}$$

where $R(s) = G_{r1}(s) + G_{r2}(s)$. From Figure 5, the transfer function from $d_{\text{qe}}^{\text{total}}$ to Δd_q is

$$G_{d\Delta}(s) = [1 + H(s)W(s)]^{-1}. \tag{24}$$

In general, we select ω_q to be five times larger than ω_{ar} such that Eq. (17) holds. As a result, the amplitude of $H(s)$ is relatively large at low frequencies as its denominator contains $[1 - F(s)]$. On the other hand, the gain of $R(s)$ is very large at the specified frequencies due to the characteristics of QRCs. Therefore, it is easy to obtain

$$| H(\mathrm{j}\omega)W(\mathrm{j}\omega) | \gg 1, \tag{25}$$

and

$$|G_{d\Delta}(\mathrm{j}\omega)| \approx 0, \tag{26}$$

at low frequencies and specified frequencies. This blocks the disturbances with frequencies that stay within the bandwidth of $F(s)$ or $R(s)$ to be transmitted to the output.

Figure 6 shows the frequency responses of the $G_{d\Delta}(s)$, $G_{r1}(s)$ and $G_{r2}(s)$ with $K_r = 200$, $\omega_c = 0.5$ rad/s, $\omega_{r1} = 30\pi$ rad/s, and $\omega_{r2} = 180\pi$ rad/s. Compared to the conventional EID estimator, the sensitivity of the EEID estimator is reduced largely in the bandwidths of $G_{r1}(s)$ and $G_{r2}(s)$, which improves disturbance-rejection performance at specified frequencies. In addition, Figure 6(a) shows that the QRCs have high gains at the specified frequencies, and thus the disturbances with these frequencies can be effectively estimated.

3.3 Stability analysis

Figure 5 shows that the closed-loop system is divided into two subsystems: the disturbance-rejection subsystem above the dashed line and the current-tracking subsystem below the line. The stability of the

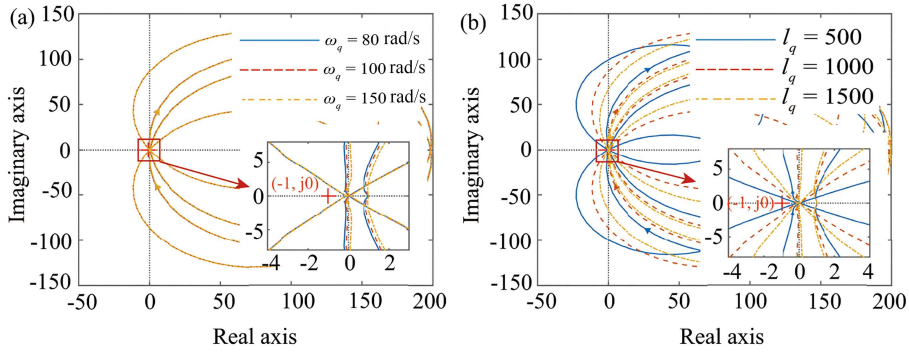

Figure 7 (Color online) Nyquist curves of the disturbance-rejection subsystem for different values of (a) ω_q and (b) l_q with $K_r = 200$, $\omega_c = 0.5$ rad/s, $\omega_{r1} = 30\pi$ rad/s, and $\omega_{r2} = 180\pi$ rad/s.

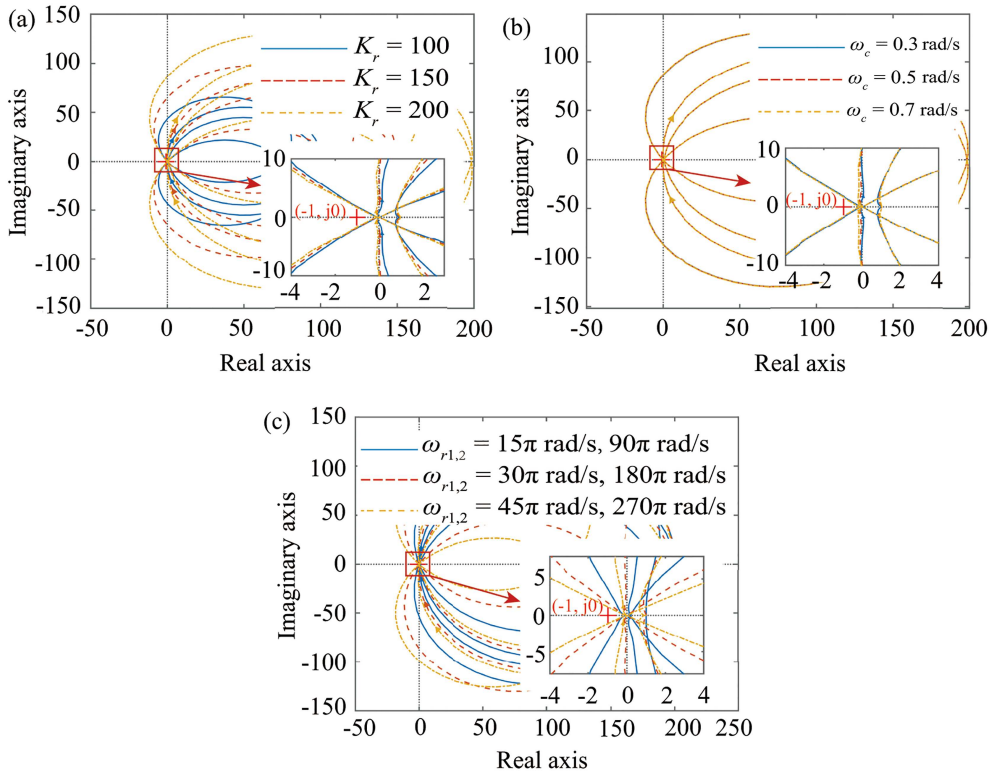

Figure 8 (Color online) Nyquist curves of the disturbance-rejection subsystem for different values of (a) K_r, (b) ω_c, (c) ω_{r1} and ω_{r2} with $l_q = 1000$, $\omega_q = 100$ rad/s.

disturbance-rejection subsystem is not affected by the current-tracking subsystem, and vice versa if the disturbance-rejection subsystem is stable. Since the stability of the current-tracking subsystem is easily guaranteed by the PI control, we mainly analyze the stability of the disturbance-rejection subsystem.

The open-loop transfer function of the disturbance-rejection subsystem, which is the transfer function from $d_{\mathrm{qe}}^{\mathrm{total}}$ to $\tilde{d}_q^{\mathrm{total}}$, is

$$G_{\mathrm{or}}(s) = \frac{l_q[F(s) + R(s)]}{(s + l_q)[1 - F(s)]}. \tag{27}$$

The stability is related to six parameters, which are the cut-off frequency ω_q, the observer gain l_q, the resonant coefficient K_r, the resonant frequencies ω_{r1} and ω_{r2}, and the resonant bandwidth ω_c. The influence of the six parameters on the stability of the system is discussed below based on the Nyquist stability criterion.

Figures 7 and 8 show the Nyquist curves of the disturbance-rejection subsystem with different values of the six parameters. The trend of the curve is analyzed to investigate the influence of the parameters on the system stability by changing one parameter and fixing the other five each time. From Figures 7 and 8,

the Nyquist curves never contain the key point $(-1, \mathrm{j}0)$, no matter what the parameters ω_q, l_q, K_r, ω_{r1}, ω_{r2}, and ω_c change. Therefore, it can be concluded that the six parameters do not affect the stability of the disturbance-rejection subsystem. However, these parameters influence the performance of the subsystem, that is, ω_q and l_q will affect the disturbance-rejection capability of the aperiodic disturbance, while K_r, ω_{r1}, ω_{r2}, and ω_c affect the current harmonic suppression performance.

The parameters do not affect the stability of the disturbance-rejection subsystem. The current-tracking subsystem is regulated by a PI controller, and its stability is easily guaranteed. As a result, the EEID-based q-axis current loop system is stable.

3.4 Parameter tuning principles

There are six parameters to be designed: the cut-off frequency ω_q, the observer gain l_q, the resonant coefficient K_r, the resonant bandwidth ω_c, and the resonant frequencies ω_{r1} and ω_{r2}. Since the integrated QRCs can be considered as an additional part to the EID estimator, we divide the above six parameters into two groups: (1) the parameters of the EID estimator (ω_q and l_q); (2) the parameters of QRCs (K_r, ω_{r1}, ω_{r1}, and ω_c). The tuning principles are explained below.

(1) First, select an angular-frequency band Ω_r for disturbance rejection at low frequencies. Next, choose ω_q of the LPF to make

$$F(\mathrm{j}\omega) \approx 1, \forall \omega \in \Omega_r \tag{28}$$

hold. Then, the pole-placement method is used to design the observer gain l_q to ensure that the bandwidth of the observer is greater than or equal to that of the LPF.

(2) Set ω_{r1} and ω_{r2} to be the frequencies of the periodic disturbances. The gain and the bandwidth of QRCs are determined by the parameters K_r and ω_c, respectively. Select a K_r to achieve satisfactory disturbance-rejection performance for the periodic disturbances. Although increasing K_r can improve the performance, it may over-amplify measurement noise at high frequencies. Choose a ω_c to obtain a desired bandwidth of the QRCs for periodic-disturbance rejection. Note that selecting a large ω_c can decrease the effectiveness of harmonic suppression.

Remark 3. The presented EEID estimator handles the periodic disturbances with known frequencies and the aperiodic disturbances with unknown frequencies. The design of the LPF in the estimator requires the bandwidth of the unknown aperiodic disturbances, which is unavailable in practice. However, the frequency range of unknown aperiodic disturbances may be available in many industrial systems. Therefore, it is reasonable to select a proper upper bound of the frequency range. The bandwidth of the LPF is usually set to be five times larger than the selected upper bound. This makes the frequencies of aperiodic disturbances stay within the bandwidth of the LPF as much as possible. On the other hand, this paper deals with periodic disturbances with known frequencies, which are used to design the QRCs in the EEID estimator. If the frequency of a periodic disturbance is not available, an adaptive algorithm can be first used to estimate its frequency in a real-time fashion. Then, the parameters of the QRC can be adapted based on the estimated frequency. This issue will be one of the directions for our future work.

4 Simulation verification

The validity and effectiveness of the proposed scheme were verified using a PMSM system. The control strategy "$i_d = 0$" was employed in the d-axis current loop and the proposed scheme was used to reject disturbances in the q-axis current loop. Figure 9 shows the block diagram of the EEID-based control scheme for the PMSM drive system.

The following disturbance, as shown in Figure 10,

$$d(t) = 3.52t + 15.2\sin 30\pi t + 4.5\sin 180\pi t + 3.4 \tag{29}$$

was imposed on the control input channel of the q-axis current loop. Simulations were carried out using the four control schemes (Table 1) for comparison.

The RC-EID approach mentioned in Table 1 is an improved EID method proposed by Mei et al. [18]. It integrated a repetitive controller into the conventional EID estimator to improve the performance of the estimator on rejecting periodic disturbances. The block diagram of the q-axis current loop using the RC-EID approach is shown in Figure 11.

The principles of parameter selection for these four methods are as follows.

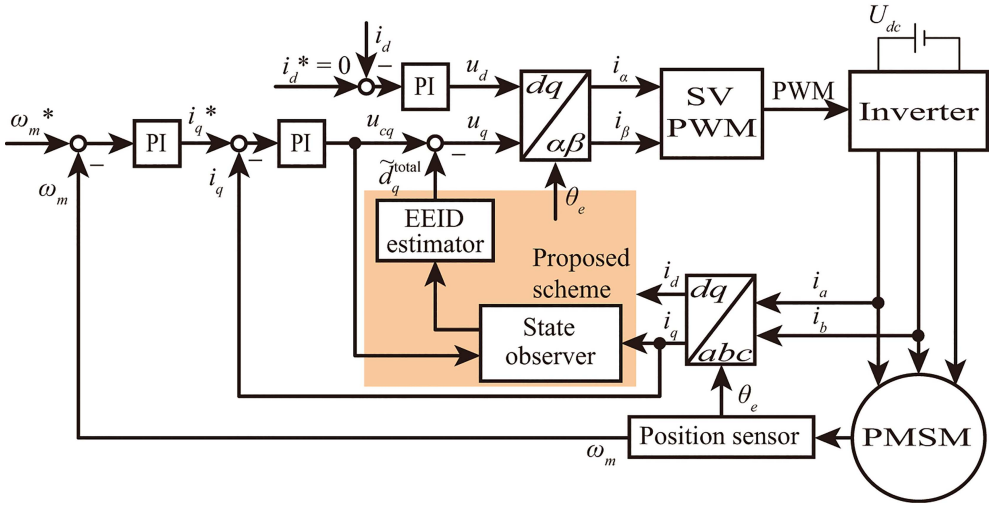

Figure 9 (Color online) Block diagram of EEID-based control scheme for the PMSM system.

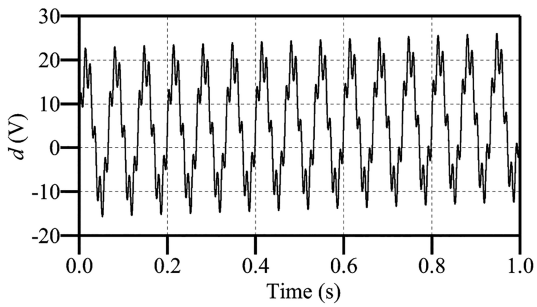

Figure 10 $d(t)$ for simulation.

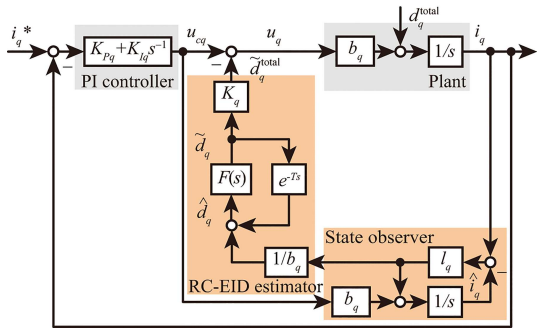

Figure 11 (Color online) Block diagram of RC-EID-based control scheme for the q-axis current loop.

Table 1 Control schemes.

Scheme	Control method
1	PI controller (PI)
2	PI controller with EID approach (PI+EID)
3	Proposed scheme (PI+EEID)
4	PI controller with RC-EID approach (PI+RC-EID)

(1) Since the four methods all contain a PI controller, the first principle of parameter selection is to choose the same gains of the PI controller for them.

(2) The PI+EID and PI+EEID methods both use an EID estimator to handle aperiodic disturbances. Thus, the second principle is to select the same parameters of the EID estimator for these two methods.

(3) The PI+RC-EID method employs the internal model to reject a periodic disturbance, while the PI+EEID method uses QRCs to do that. Since the gain K_q in the RC-EID estimator plays a similar role to the gain K_r in the EEID estimator, the third principle is that K_r and K_q are set to be the same.

The same scenario of the PI control in [2] was used in this study, that is, the parameters of the PI controller in the speed loop were $K_{\text{P}\omega} = 0.05$, $K_{\text{I}\omega} = 0.28$; those in the d-axis current loop were $K_{\text{Pd}} = 11.2$, $K_{\text{Id}} = 1047.5$; and those in the q-axis current loop were $K_{\text{Pq}} = 13.2$, $K_{\text{Iq}} = 1083.5$.

The parameters of the QRCs were set to $K_r = 200$, $\omega_c = 0.5$ rad/s, $\omega_{r1} = 30\pi$ rad/s, and $\omega_{r2} = 180\pi$ rad/s. The bandwidth ω_q of the LPF was chosen to be 100 rad/s. The gain of the observer was set to be 1000. The bandwidth of the filter and the gain of the state observer used in the RC-EID estimator were set to be the same as those in the presented method. As a result, the parameters in the RC-EID estimator were $K_q = 200$ and $T = 0.067$ s. The reference speed was set to be 300 r/min. The parameters of the PMSM for simulation are shown in Table 2.

Table 2 Parameters of the PMSM for simulations.

Symbol	Description	Value
p_n	Number of pole pairs	4
R_s	Stator resistance	0.985 Ω
ψ_f	Flux linkage	0.1827 Wb
L_d, L_q	d- and q-axis inductance	12 mH
J	Moment of inertia	0.003 Kg · m^2

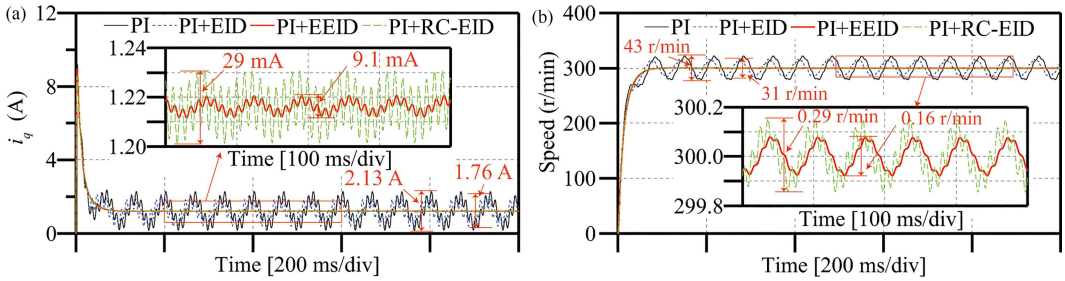

Figure 12 (Color online) Simulation results of the outputs of (a) the current and (b) speed.

Table 3 Performance assessment for three methods.

Method	IAE$_D$	IAE$_Y$	ITAE$_Y$
Conventional EID	2.9490	3.7440	2.6070
RC-EID	0.0391	0.0266	0.0187
EEID	0.0177	0.0179	0.0125

Figure 12 shows the simulation results of the outputs of the current and speed for the methods. The periodic disturbance had a significant effect on the current and speed when the PI and PI+EID methods were used. The peak-to-peak tracking errors in the current and the speed were about 2.13 A and about 43 r/min respectively for the PI method. They were reduced to about 1.76 A and 31 r/min for the PI+EID method. It indicates that the conventional EID estimator has a limited ability to handle periodic disturbances as there are still obvious periodic fluctuations in the outputs of the current and speed. In contrast, the current and speed ripples were effectively suppressed for the PI+EEID and PI+RC-EID methods. Moreover, the presented PI+EEID method yielded a bigger improvement than the PI+RC-EID did. The errors were 9.1 mA and 0.16 r/min for the presented method, which were 31.4% and 55.2% of those for the PI+RC-EID method. Therefore, the proposed scheme has a better disturbance-rejection performance than the other three methods.

To provide a quantitative analysis of the comparison, we calculate the following performance indices: the integral of absolute error (IAE) and the integral of time-weighted absolute error (ITAE) in the output, and the IAE in disturbance estimation. These indices are denoted by

$$\begin{cases} \text{IAE}_D = \displaystyle\int_{0.5}^{0.9} \left| d_q^{\text{total}}(t) - \tilde{d}_q^{\text{total}}(t) \right| \mathrm{d}t, \\ \text{IAE}_Y = \displaystyle\int_{0.5}^{0.9} \left| \omega_m(t) - \omega^*(t) \right| \mathrm{d}t, \\ \text{ITAE}_Y = \displaystyle\int_{0.5}^{0.9} t \left| \omega_m(t) - \omega^*(t) \right| \mathrm{d}t. \end{cases} \tag{30}$$

The results are shown in Table 3. It indicates that the performance of the EEID approach is better than that of the other methods.

Figure 13 shows simulation results of disturbance estimation for the conventional EID, EEID, and RC-EID estimators. The component of the disturbance with 180π rad/s cannot be estimated by the conventional EID estimator as the bandwidth of the filter was only 100 rad/s. Since the QRCs in the EEID estimator and the repetitive controller in the RC-EID estimator were designed to handle the periodic disturbance, both estimators reconstructed the disturbance effectively. Moreover, the estimation error was smaller for the EEID estimator than for the RC-EID estimator. The error was 0.16 V for the EEID estimator, which was 38% of that for the RC-EID estimator.

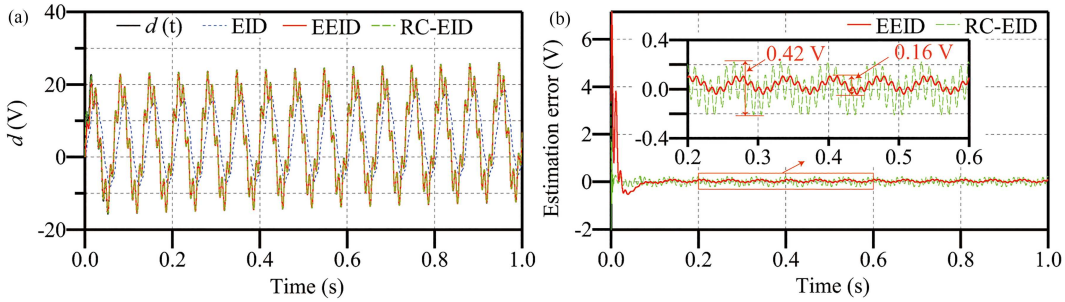

Figure 13 (Color online) Simulation results of disturbance estimation. (a) Estimates; (b) estimate errors.

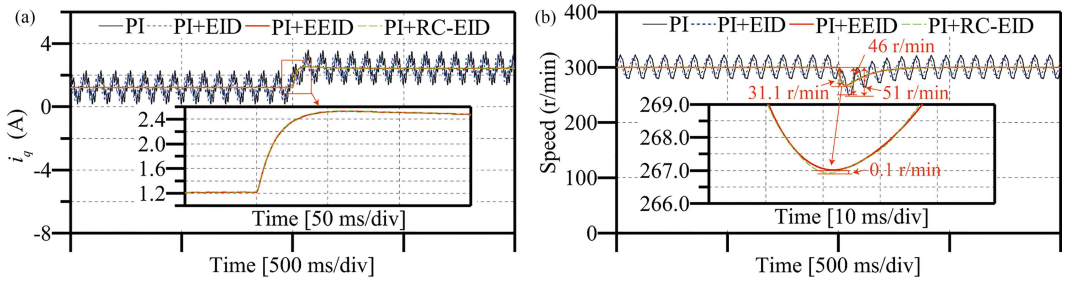

Figure 14 (Color online) Simulation results of the outputs of (a) the current and (b) speed with load torque changes.

Figure 14 shows the simulation results of the outputs of current and speed for the methods as the load torque changes. The load torque change results in a large speed drop for the PI and PI+EID methods. The speed drop was about 51 r/min for the PI method. It was reduced to about 46 r/min for the PI+EID method. This indicates that the ability of the conventional EID estimator to handle aperiodic disturbances is limited by the periodic disturbances. In contrast, the PI+EEID and PI+RC-EID methods are effective in suppressing aperiodic disturbances such as load torque changes, even in the presence of periodic disturbances. The PI+EEID and PI+RC-EID methods were able to reduce the speed drop to 31 and 31.1 r/min respectively, and the two methods were very close in dealing with the aperiodic disturbances, with an error of only about 0.1 r/min. Therefore, the proposed scheme has a better performance in suppressing both the aperiodic and periodic disturbances.

Since the main differences between simulations and experiments are measurement noise and parameter uncertainties, the noise (band-limited white noise with a power of 10^{-6} and a sampling time of 0.001 s) with a peak value of $\pm 10\%$ of the corresponding largest output was added to the output i_q. Moreover, a 10% uncertainty in the control gain b_q and a time-varying uncertainty $\Delta a_q(t)$ were introduced to the plant (2). The uncertainties are

$$\Delta a_q(t) = 0.25 \sin 0.6t, \Delta b_q = 0.1 b_q. \tag{31}$$

Figures 15 and 16 show the simulation results for the methods in the presence of the measurement noise and uncertainties. The results indicate that the presented method achieved better performance of disturbance rejection and noise suppression than the other methods did. It can be seen that the EEID estimator is robust to parameter uncertainties. Moreover, measurement noise has little effect on the estimates and output. This demonstrates that the presented method is practical.

5 Conclusion

The EEID approach has been proposed to suppress aperiodic and periodic current ripples for the current loop of a PMSM. An additional degree of periodic disturbance estimation was developed to enhance the performance by integrating QRCs into the conventional EID estimator. The analysis of disturbance-rejection performance showed that the sensitivity for disturbance rejection at the specified frequencies was reduced largely. The stability analysis indicated that the design of the system can be separated into that of two subsystems: the current-tracking subsystem and the disturbance-rejection subsystem. The simulation results demonstrated that the presented EEID estimator effectively suppressed periodic

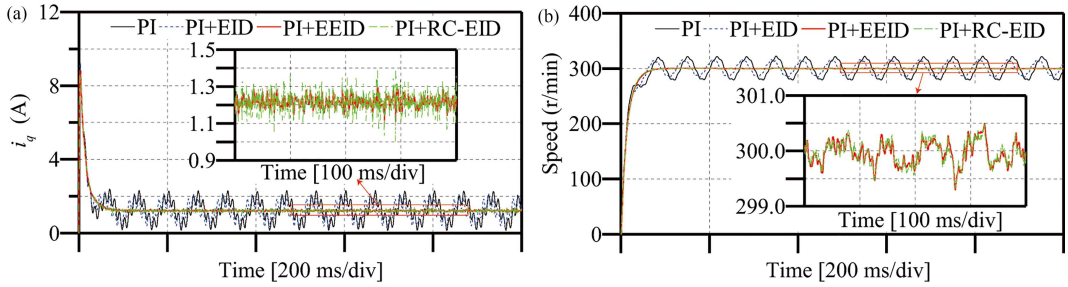

Figure 15 (Color online) Simulation results of the outputs of (a) the current and (b) speed in the presence of measurement noise and uncertainties.

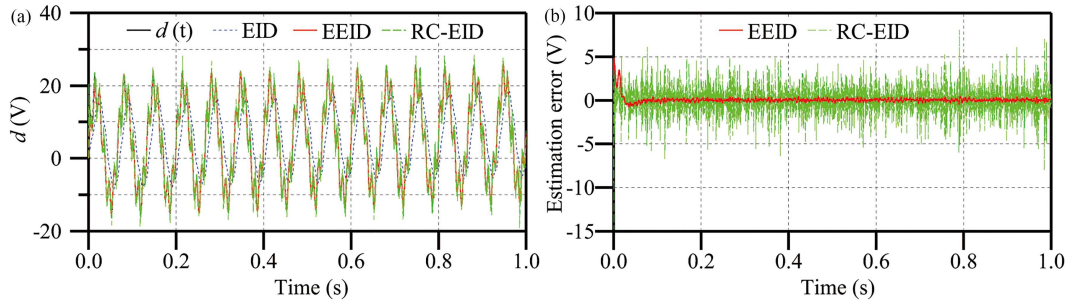

Figure 16 (Color online) Simulation results of disturbance estimation in the presence of measurement noise and uncertainties. (a) Estimates; (b) estimate errors.

disturbances, reduced current ripples, and improved control performance. The design of QRCs in the EEID estimator requires that the frequencies of the periodic disturbances should be known. However, if the frequencies are unknown, how to design the QRCs is a challenge. In addition, several noticeable issues are how to handle time delays caused by signal transmission [25]; how to extend the method to nonlinear systems [26, 27]; and how to guarantee an adequate optimal index of the overall disturbance-rejection performance. These are some directions for our future work.

Acknowledgements This work was supported in part by Natural Science Foundation of Jiangsu Province (Grant No. BK20221404), Ministry of Education Chunhui Program Collaborative Research Project of China (Grant No. 202200164), Leading Innovative Talent Introduction and Cultivation Program of Changzhou (Grant No. CQ20230079), Wuhan Applied Foundational Frontier Project (Grant No. 2020010601012175), Beijing Municipal Natural Science Foundation (Grant No. 4244089), and Zhongwu Innovative Talent Project of Jiangsu University of Technology.

References

1 Chen S, Chen Z X, Huang Y, et al. New design of active disturbance rejection control for nonlinear uncertain systems with unknown control input gain. Sci China Inf Sci, 2022, 65: 142201
2 Wang Y, Yu H, Niu S, et al. Adaptive observer-based current constraint control for electric vehicle used PMSM. Appl Energy, 2024, 360: 122802
3 Zhao K, Jia N, She J, et al. Robust model-free super-twisting sliding-mode control method based on extended sliding-mode disturbance observer for PMSM drive system. Control Eng Pract, 2023, 139: 105657
4 Chen Q, Li Y, Hong Y, et al. Prescribed-time robust repetitive learning control for PMSM servo systems. IEEE Trans Ind Electron, 2024, 71: 14753–14763
5 Kurniawan E, Harno H G, Wang H, et al. Robust adaptive repetitive control for unknown linear systems with odd-harmonic periodic disturbances. Sci China Inf Sci, 2022, 65: 222202
6 Yang J, Chen W H, Li S, et al. Disturbance/uncertainty estimation and attenuation techniques in PMSM drives — a survey. IEEE Trans Ind Electron, 2017, 64: 3273–3285
7 Cai W, She J, Wu M, et al. Disturbance suppression for quadrotor UAV using sliding-mode-observer-based equivalent-input-disturbance approach. ISA Trans, 2019, 92: 286–297
8 Xu J, Wei Z, Wang S. Active disturbance rejection repetitive control for current harmonic suppression of PMSM. IEEE Trans Power Electron, 2023, 38: 14423–14437
9 Pejovski D, Gerlando A D, Foglia G M, et al. Current harmonics in surface-mounted PMSM electrical drive for monitoring torsional vibrations. IEEE Trans Ind Appl, 2024, 60: 3840–3849
10 Mohamed Y A R I. Design and implementation of a robust current-control scheme for a PMSM vector drive with a simple adaptive disturbance observer. IEEE Trans Ind Electron, 2007, 54: 1981–1988
11 Du Y, She J, Cao W. Improving performance of disturbance rejection for nonlinear systems using improved equivalent-input-disturbance approach. IEEE Trans Ind Inf, 2024, 20: 941–952
12 Du Y, Cao W, She J, et al. Analysis and robust control of system with uncertainty and disturbance using equivalent-input-disturbance approach. J Franklin Inst, 2023, 360: 4675–4694
13 Godbole A A, Kolhe J P, Talole S E. Performance analysis of generalized extended state observer in tackling sinusoidal disturbances. IEEE Trans Contr Syst Technol, 2013, 21: 2212–2223
14 Pukdeboon C. Extended state observer-based third-order sliding mode finite-time attitude tracking controller for rigid spacecraft. Sci China Inf Sci, 2019, 62: 12206

15 Tang Z, Akin B. Suppression of dead-time distortion through revised repetitive controller in PMSM drives. IEEE Trans Energy Convers, 2017, 32: 918–930
16 Hu M, Hua W, Ma G, et al. Improved current dynamics of proportional-integral-resonant controller for a dual three-phase FSPM machine. IEEE Trans Ind Electron, 2021, 68: 11719–11730
17 Li H, Bai J, Zou H, et al. A two-dimensional model predictive iterative learning control based on the set point learning strategy for batch processes. J Process Control, 2024, 133: 103133
18 Mei Q C, She J H, Liu Z T, et al. Estimation and compensation of periodic disturbance using internal-model-based equivalent-input-disturbance approach. Sci China Inf Sci, 2022, 65: 182205
19 Mohanapriya S, Sakthivel R, Almakhles D J. Design of robust tracking and disturbance attenuation control for stochastic control systems. ISA Trans, 2022, 129: 110–120
20 Wang B, Tian M, Yu Y, et al. Enhanced ADRC with quasi-resonant control for PMSM speed regulation considering aperiodic and periodic disturbances. IEEE Trans Transp Electrific, 2022, 8: 3568–3577
21 Xia C, Ji B, Yan Y. Smooth speed control for low-speed high-torque permanent-magnet synchronous motor using proportional-integral-resonant controller. IEEE Trans Ind Electron, 2015, 62: 2123–2134
22 Huang D, Min D, Jian Y, et al. Current-cycle iterative learning control for high-precision position tracking of piezoelectric actuator system via active disturbance rejection control for hysteresis compensation. IEEE Trans Ind Electron, 2020, 67: 8680–8690
23 Liu X, Deng Y, Wang J, et al. Fixed-time generalized active disturbance rejection with quasi-resonant control for PMSM speed disturbances suppression. IEEE Trans Power Electron, 2024, 39: 6903–6918
24 Zhang X, Cao Y, Zhang C. Model predictive voltage control for PMSM system with low parameter sensitivity. IEEE Trans Ind Electron, 2024, 71: 13601–13613
25 Kwon O M, Lee S H, Park M J. Some novel results on stability analysis of generalized neural networks with time-varying delays via augmented approach. IEEE Trans Cybern, 2022, 52: 2238–2248
26 Selvaraj P, Kwon O M, Lee S H, et al. Disturbance rejections of polynomial fuzzy systems under equivalent-input-disturbance estimator approach. Fuzzy Sets Syst, 2024, 488: 109013
27 Selvaraj P, Kwon O M, Lee S H, et al. Disturbance rejections of interval type-2 fuzzy systems under event-triggered control scheme. Appl Math Comput, 2022, 431: 127323